Apaf-1 deficiency and neural tube closure defects are found in *fog* mice

Narimon Honarpour*, Sandra L. Gilbert†‡, Bruce T. Lahn†‡, Xiaodong Wang§¶, and Joachim Herz*‖

Departments of *Molecular Genetics and §Biochemistry, and ¶Howard Hughes Medical Institute, The University of Texas Southwestern Medical Center, Dallas, TX 75390-9046; and †Department of Human Genetics, and ††Howard Hughes Medical Institute, University of Chicago, Chicago, IL 60637

Communicated by Ronald W. Estabrook, University of Texas Southwestern Medical Center, Dallas, TX, June 6, 2001 (received for review April 2, 2001)

The forebrain overgrowth mutation (*fog*) was originally described as a spontaneous autosomal recessive mutation mapping to mouse chromosome 10 that produces forebrain defects, facial defects, and spina bifida. Although the *fog* mutant has been characterized and available to investigators for several years, the underlying mutation causing the pathology has not been known. Because of its phenotypic resemblance to apoptotic protease activating factor-1 (Apaf-1) knockout mice, we have investigated the possibility that the *fog* mutation is in the *Apaf-1* gene. Allelic complementation, Western blot analysis, and caspase activation assays indicate that *fog* mutant mice lack Apaf-1 activity. Northern blot and reverse transcription-PCR analysis show that *Apaf-1* mRNA is aberrantly processed, resulting in greatly reduced expression levels of normal *Apaf-1* mRNA. These findings are strongly suggestive of the *fog* mutation being a hypomorphic *Apaf-1* defect and implicate neural progenitor cell death in the pathogenesis of spina bifida—a common human congenital malformation. Because a complete deficiency in *Apaf-1* usually results in perinatal lethality and *fog*/*fog* mice more readily survive into adulthood, these mutants serve as a valuable model with which apoptotic cell death can be studied *in vivo*.

spina bifida | neural development | apoptosis | caspase | cell death

Neural tube closure defects account for a significant portion of the congenital malformations that affect humans (1). Such defects include spina bifida, exencephaly, cranioschisis, and hydrocephaly. The cause and inheritance of these defects are complex, reflecting the complex developmental events required for neural tube formation and closure.

Neural plate formation, neural fold elevation, neural tube closure, and neural crest cell migration are just a few of the operations that are tightly regulated during neurulation. Many mouse models have been used to study neural tube defects (2). The mutants studied have either arisen spontaneously or have been generated by using targeted gene disruption. One such mouse model is the forebrain overgrowth (*fog*) mutant, which has a spontaneous mutation in an uncharacterized gene and is transmitted in an autosomal recessive manner (3).

Apoptotic cell death has been shown to play a critical role in neurogenesis. Specifically, proteins required for the cytochrome-*c*-mediated apoptotic pathway [such as apoptotic protease activating factor-1 (Apaf-1), caspase-9, and caspase-3] are important for neural tube closure *in vivo* (4–9). In this biochemical cascade, cytochrome *c* released from the mitochondria is recruited to Apaf-1. In the presence of dATP, the cytochrome-*c*/Apaf-1 complex is able to procure and promote activation of procaspase-9 to caspase-9. The activation of caspase-9 then results in the subsequent activation of caspase-3, a terminal event in apoptotic cell death. In mice, *Apaf-1* deficiency results in a dramatic elevation in the number of neural progenitor cells resulting in the thickening of the neuroepithelium (9). Because morphogenetic forces play a critical role in neurulation (10), it is likely that the abundance of neural progenitors in *Apaf-1* mutants profoundly affects the ability of the neural tube to close. Given that apoptotic cell death is crucial for appropriate neural development, uncharacterized mutant models that are used to study neurulation may possess defects in apoptotic programs. In this study, we show that mice with the *fog* mutation are functionally deficient in Apaf-1 protein. We find that *Apaf-1* transcripts are aberrantly processed in homozygous *fog* mutants, resulting in reduced levels of the normal *Apaf-1* message. In addition to the phenotypes that have been previously reported for the *Apaf-1* knockouts generated by targeted gene disruption, the *fog* mutants frequently have spina bifida and some surviving adult animals have typical neural tube closure defects (3). These findings suggest that the degree of *Apaf-1* expression is critical in the regulation of neural progenitor cell death, and that perturbations in this regulation result in neurodevelopmental pathology such as spina bifida.

Materials and Methods

Mapping of the *Apaf-1* Allele. Polymorphisms between the *Apaf-1* alleles of C57BL/6J and SPRET mice were identified by sequencing the 3′ end of the locus. This revealed a 10-bp allelic size difference within the 3′ untranslated region (UTR). The following PCR primers were designed to generate a product that spans the polymorphism: Apaf-1-gap-F: 5′-CTATGAGCTAGTCATGTGTTAGA-3′ and Apaf1-gap-R: 5′-CCAATTCACAGACACTGACA-3′. Genomic DNA samples derived from 94 N2 animals from the BSS backcrosses (C57BL/6JEi × SPRET/Ei)F_1 × SPRET/Ei, or the reciprocal BSB backcrosses (C57BL/6JEi × SPRET/Ei)F_1 × C57BL/6JEi were analyzed by PCR for the 3′ UTR polymorphism. PCR was performed in a 20-μl volume that contained 1.5 mM $MgCl_2$, 50 mM KCl, 10 mM Tris (pH 9.0), 1% Triton X-100, 0.5 μM each primer, 0.1 mM dNTPs, 1 unit of *Taq* DNA polymerase, and 25 ng of genomic DNA. After denaturation at 95°C for 1.5 min, 30 cycles of PCR were performed where each cycle consisted of 1 min at 95°C, 45 sec at 60°C, and 45 sec at 72°C. Products were then resolved on 4% NuSieve agarose (FMC) gels. The results were then compared with The Jackson Laboratory Backcross Database (available at http://www.jax.org/resources/documents/cmdata; see also http://www.informatics.jax.org/).

Generation of *Apaf-1* Knockout Mice. Mice carrying the disrupted *Apaf-1* allele were generated as described (9). Mice carrying the *fog* mutation were obtained from The Jackson Laboratory (stock no. 002979). Embryos possessing one disrupted *Apaf-1* allele and one *fog* mutant allele were obtained by crossing male mice heterozygous for the *fog* mutation with females heterozygous for a disrupted *Apaf-1* allele.

Histology. Specimens were fixed in 4% paraformaldehyde overnight and subsequently embedded in paraffin for sectioning.

DEVELOPMENTAL BIOLOGY

Abbreviations: Apaf-1, apoptotic protease activating factor-1; RT, reverse transcription; cM, centimorgan.

‖To whom reprint requests should be addressed. E-mail: herz@utsw.swmed.edu.

The publication costs of this article were defrayed in part by page charge payment. This article must therefore be hereby marked "*advertisement*" in accordance with 18 U.S.C. §1734 solely to indicate this fact.

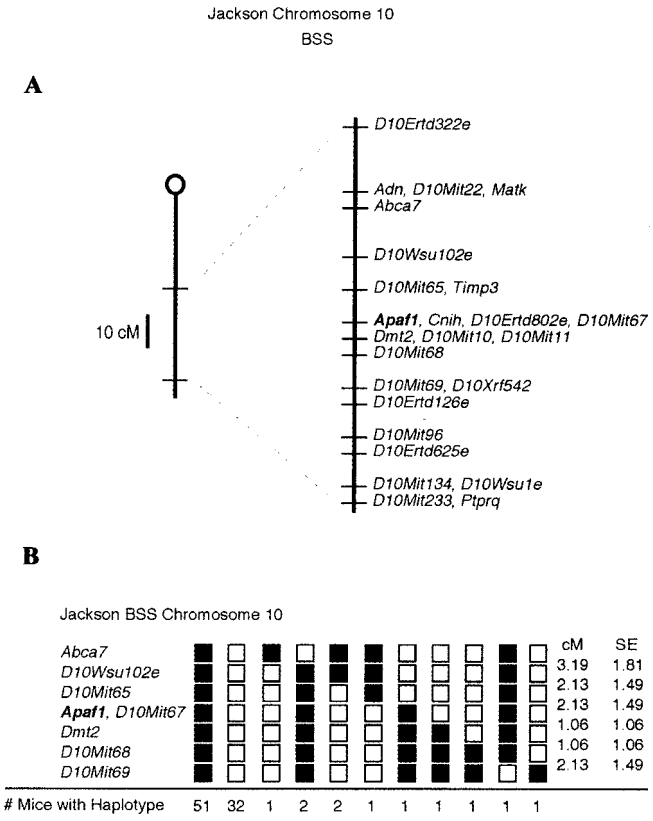

Fig. 1. Partial chromosomal linkage map showing mouse chromosome 10 with loci linked to *Apaf-1*. (*A*) *Apaf-1* maps 45.7 centimorgan (cM) distal to the centromere of mouse chromosome 10 by using the Jackson Laboratory interspecific backcross panel BSS. Ninety-four of the (C57BL/6JEi × SPRET/Ei)F_1 × SPRET/Ei progeny were typed for inheritance of the *Mus domesticus* or *Mus spretus* alleles. The Jackson BSS map is depicted with the centromere toward the top. A 10 cM scale bar is shown to the left of the figure. Loci that map to the same position are listed in alphabetical order. (*B*) The loci linked to *Apaf-1* are listed in order with the most proximal at the top. Black boxes represent the *M. domesticus* allele, and white boxes depict the *M. spretus* allele. For each haplotype, the number of animals in the BSS panel displaying that haplotype is listed below each column of boxes. The percent recombination between adjacent loci is listed in cM to the right of the figure, along with the SE. Raw data from The Jackson Laboratory were obtained from the World Wide Web address http://www.jax.org/resources/documents/cmdata.

Sections were cut at 5-μm increments, and stained with hematoxylin/eosin.

Preparation of S-100 Extracts from Fibroblasts. Mouse embryonic fibroblasts derived from day 16.5 embryos were prepared and maintained by using the procedure outlined (11). Primary fibroblast cultures were derived from the adult mouse tail. Pieces of the tissue were allowed to adhere to 25-cm^2 flasks and were incubated in Dulbecco's modified media (high glucose with glutamine) supplemented with 20% FCS and penicillin/streptomycin. Fibroblasts were harvested and collected by centrifugation (1,800 × *g* for 15 min at 4°C). Cell pellets were washed once with ice-cold PBS and resuspended in 5 vol of ice-cold buffer A (20 mM Hepes, pH 7.5/10 mM KCl/1.5 mM $MgCl_2$/1 mM NaEDTA/1 mM DTT/0.1 mM PMSF). After 15 min of incubation on ice, cells were homogenized with 20 strokes of a Dounce homogenizer. After centrifugation (2,000 × *g*, 5 min at 4°C) the supernatant was collected and centrifuged again (100,000 × *g*, 1 h at 4°C). The resulting supernatant (S-100 extract) was stored at −80°C.

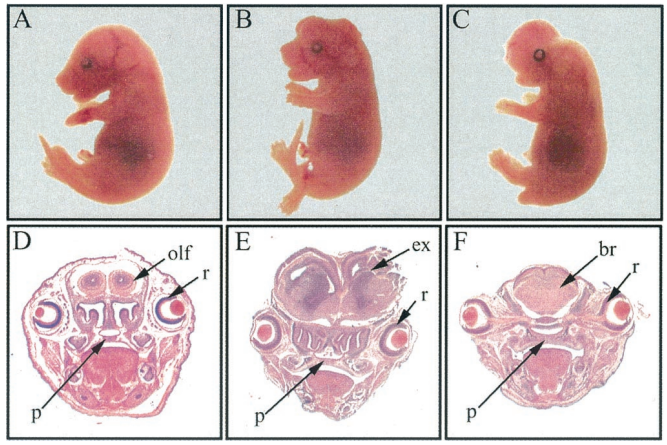

Fig. 2. Embryonic day 16.5 pups derived from *Apaf-1* +/−; *fog*/+ crosses possess a mutant phenotype. (*A*) The phenotype of a wild-type pup. (*B* and *C*) The phenotypes of the mutant pups obtained. The phenotypes seen in the head region closely resemble those seen in *fog*/*fog* and *Apaf-1* −/− newborns. (*D*) A wild-type embryo at a level analogous to that shown for the mutants. (*E* and *F*) Histological sections from the mutant pups shown in *B* and *C*. Note that the histological findings in these animals mimic those of the *Apaf-1* knockout. olf, Olfactory bulb; br, poorly organized brain tissue in a mutant with cranioschesis; ex, exencephalic brain tissue; p, palate; r, retina.

Immunoblot Analysis. Western blot analysis of Apaf-1 was performed as described (12). Immunoblot analysis was performed by using horseradish peroxidase-conjugated goat anti-rabbit IgG and enhanced chemiluminescence (ECL) Western blotting detection reagents (Amersham Pharmacia).

***In Vitro* Caspase-3 Activation Assay.** Procaspase-3 was translated *in vitro* and purified as described (13). A 1-μl aliquot of the *in vitro*

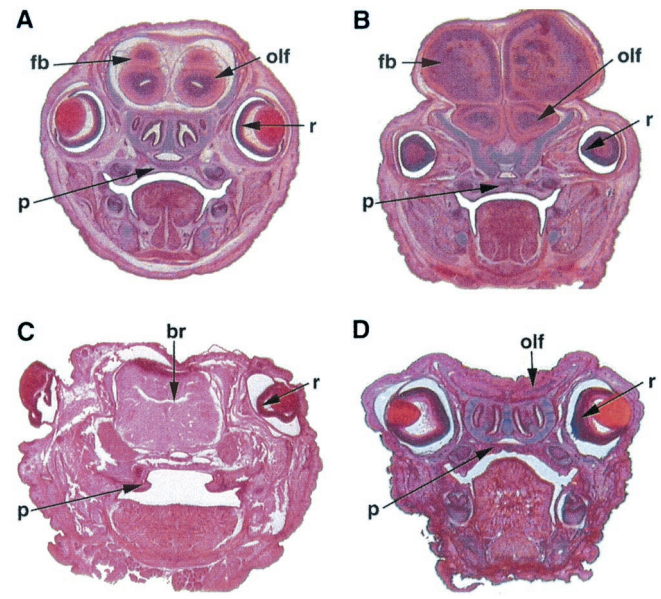

Fig. 3. Phenotypic variation in *Apaf-1*-deficient newborns closely resembles that seen in *fog* embryos. (*A*) A wild-type littermate. In the mutant shown in *B*, the generalized hypercellularity of the forebrain and basal ganglionic region results in exencephaly with compression and narrowing of the ventricles. Midline closure defects involving the palate and nasal septum are also seen in *Apaf-1* mutant pups, and in extreme cases cranioschesis (as seen in *C*) occurs. (*D*) An anencephalic *Apaf-1* mutant newborn. The telencephalon, mesencephalon, and diencephalon are absent, but remnants of the olfactory nerves remain. fb, Forebrain; olf, olfactory bulbs; p, palate; r, retina; br, poorly organized brain tissue.

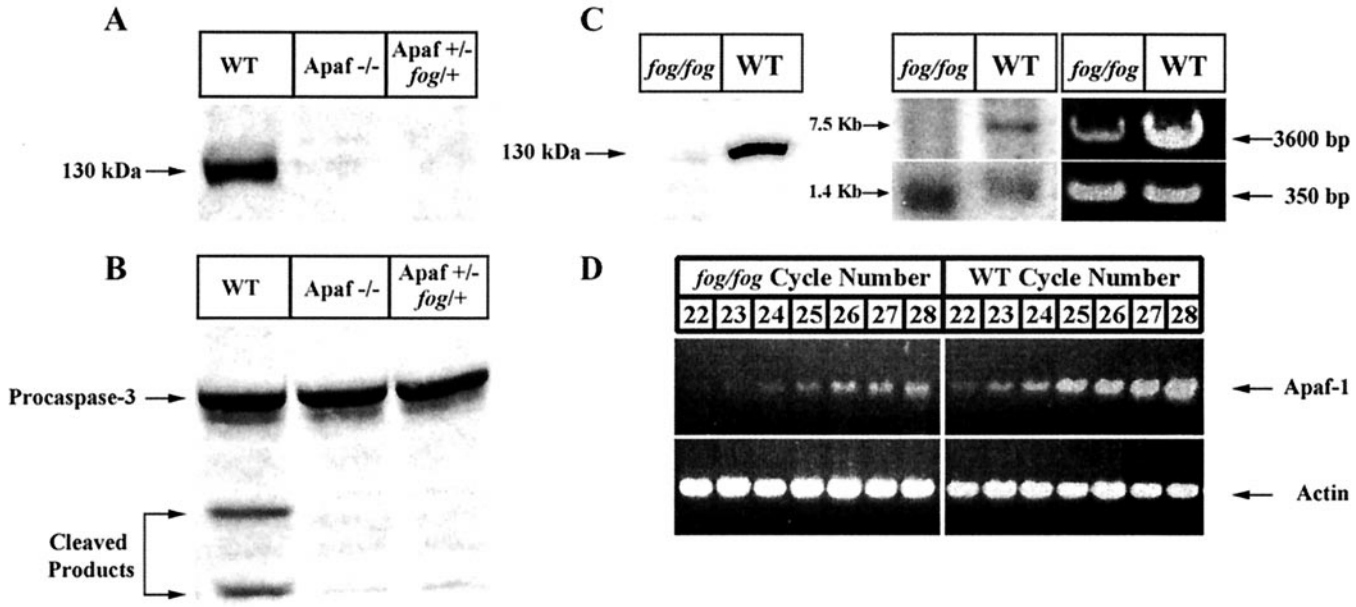

Fig. 4. Biochemical analysis of fibroblasts derived from mutant pups and *fog/fog* fibroblasts. (*A*) Fibroblast extracts derived from the mutant pups of the *Apaf-1* +/−, *fog*/+ cross are compared with extracts derived from wild-type and *Apaf-1* knockout mouse embryonic fibroblasts for reactivity to an antibody directed against Apaf-1. No detectable Apaf-1 (130 kDa in mass) is seen in the lane loaded with extracts from the fibroblasts of the mutant pup or from the *Apaf-1*-deficient pup. (*B*) The same extracts from *A* are tested for the ability to cleave ^{35}S-labeled caspase-3 *in vitro*. Although extracts from wild-type fibroblasts are able to cleave procaspase-3, extracts from the mutant fibroblasts and Apaf-1-deficient fibroblasts fail to cleave and activate procaspase-3. (*C*) Protein and RNA prepared from fibroblasts of wild-type mice (WT) and mice homozygous for the *fog* mutation (*fog/fog*) were analyzed by using Western blot analysis (left), Northern blot analysis (center), and RT-PCR (right). No detectable Apaf-1 protein (130 kDa) or mRNA (7.5 kb) is present in *fog/fog* samples. Cyclophilin mRNA was probed on the same blot and used as a loading control (1.4 kb). Primer pairs used for RT-PCR (spanning all but 70 bp of the *Apaf-1* cDNA) amplify a 3,600-bp fragment in the *fog/fog* sample but at a reduced level. This indicates that *Apaf-1* message is present at significantly reduced quantities in *fog* mutants (the β-actin product running at 350 bp is shown as a positive control). (*D*) RT-PCR is used to amplify a fragment (primer pair 1 and 14) spanning exons 2 through 4 of *Apaf-1* from *fog/fog* and wild-type first-strand cDNA. The product is less abundant and appears in higher PCR cycle numbers in *fog/fog* samples relative to wild-type samples.

translated procaspase-3 was incubated with 50 μg of cell extract in the presence or absence of 1 mM dATP and 1 mM $MgCl_2$ at 30°C for 1 h. Before incubation, the volume was adjusted to 20 μl with buffer A. After incubation, 7 μl of 4× SDS sample buffer was added, samples were then boiled for 3 min, and then subjected to SDS/15% PAGE. The gel was transferred to a nitrocellulose filter, and ^{35}S-labeled protein bands were visualized on a Fuji BAS-1500 phosphorimager.

Reverse Transcription (RT)-PCR. Total RNA was purified from mouse embryonic fibroblasts by using the RNA-STAT-60 RNA isolation reagent. The total RNA was used to generate first-strand cDNA by using the SuperScript II reverse transcriptase kit and oligo(dT) primer available from Life Technologies. The first-strand cDNA was used for amplifying fragments of the *Apaf-1* message. Oligonucleotides used in amplifying the aberrantly spliced *Apaf-1* message from the first strand cDNA were the 1 and 13 primers, which have the sequence 5′-CATCAAGACATCCTACATCATGGATCACATG-3′ and 5′-GGTACTCCACCTTCACACAGCACTG-3′ respectively. Nearly full-length transcripts were amplified with the 1 primer and the 11 primer, 5′-CCGAGATTATCGACAGTCACATAGG-3′. The remainder of the coding region was amplified by using primers with the reverse complement sequence of 1 and 11 with the primers 5′-GCAATCTAGTCTCATAAGTGACCCTC-3′ and 5′-GGGTCAAGCTCAGTCGAGTATAACT-3′, respectively. PCR used to quantify the difference in *Apaf-1* message between *fog* mutants and wild-type animals used primer pair 1 and 14, 5′-TCATGAGAAGCCCAGATTTGTCTTG-3′. β-Actin message was amplified by using primers provided with the RT-PCR Primer and Control Set kit from Life Technologies.

Northern Analysis. Northern blots were performed as described (14). Total RNA obtained from cultured fibroblasts was eluted over an oligo(dT) column (mRNA purification kit, Amersham Pharmacia), and ≈5 μg of resulting RNA preparation was loaded per well. The blots were probed with a ^{32}P-labeled fragment spanning 3,600 bp of the *Apaf-1* cDNA (amplified by the 1 and 11 primer pair).

Results

The similarity in phenotype between the *Apaf-1* −/− mice and *fog* mutant mice, as well as the proximity of both loci on mouse chromosome ten (3, 5), suggested *Apaf-1* as a candidate gene for the *fog* mutation. To determine the chromosomal localization at a higher resolution, *Apaf-1* was mapped by using two interspecific backcross mouse DNA panels from The Jackson Laboratory (15). Genomic DNA samples derived from 94 N_2 animals from the BSS backcrosses (C57BL/6JEi × SPRET/Ei)F_1 × SPRET/Ei were analyzed for a clear PCR-based polymorphic marker in the 3′ untranslated region of the *Apaf-1* locus between the two species. The segregation pattern of the polymorphism was compared with The Jackson Laboratory Backcross Database, where the marker was found to cosegregate with *D10Mit67* and closely segregate with several adjacent loci located on mouse chromosome 10 (Fig. 1). The mapping places the *Apaf-1* locus at consensus position 45.7 on mouse chromosome 10. Similar data, albeit of lower resolution, were obtained from the reciprocal BSB backcross panel (C57BL/6JEi × SPRET/Ei)F_1 × C57BL/6JEi (data not shown). Previous linkage analysis has shown that the *fog* mutant phenotype does not recombine with either *D10Mit262* [47.5 centimorgan (cM)] or *D10Mit230* (49.0

cM) (3). Thus, *Apaf-1* maps within the minimal region to which the *fog* mutation has been localized (Fig. 1).

To further evaluate the possibility that the *Apaf-1* and *fog* alleles represent the same gene, female mice heterozygous for a disrupted *Apaf-1* allele were crossed to male mice heterozygous for the *fog* mutation (obtained from The Jackson Laboratory). The pups from this cross were harvested at 16.5 days of gestation (Fig. 2). A variety of mutant phenotypes were observed, consistent with the defects reported for *fog* mutants (3) and with those seen in *Apaf-1*-deficient mice (Fig. 3). The *fog/Apaf-1* mutant phenotype included exencephaly, cranioschesis, or either forebrain defect with lumbosacral defects. *fog/fog* embryos have been reported to have similar defects in addition to lumbosacral defects alone. The relative frequency of the different phenotypes was not assessed in this experiment; the frequency of these defects has been quantified in both *fog* mutants and *Apaf-1* knockout mice (3, 6).

Western blot analysis of mouse embryonic fibroblasts derived from these mutant pups revealed an absence of Apaf-1 protein (Fig. 4*A*). Extracts prepared from these cells also failed to activate caspase-3 *in vitro*, consistent with the absence of Apaf-1 (Fig. 4*B*) (13). Furthermore, fibroblasts derived from *fog/fog* mutants had no detectable *Apaf-1* transcript or protein by Northern (Fig. 4*C Center*) or Western blot analysis (Fig. 4*C Left*), respectively. Because the *Apaf-1* message is normally expressed at low levels, there remained a possibility that even lower levels of *Apaf-1* message (undetectable by Northern analysis) were present in the *fog* mutant. To address this, RT-PCR was performed on total RNA from wild-type and *fog/fog* mutant cultured fibroblasts. This analysis indicates that *Apaf-1* transcripts are in fact present in the mutant, but are ≈10- to 20-fold less abundant (Fig. 4 *C Right* and *D*). The coding region (from start codon to stop codon) of the *Apaf-1* cDNA was sequenced by using fragments amplified from *fog/fog* first-strand cDNA, and no mutations were found when compared with wild-type animals in the C3H/HeJ background on which the *fog* mutation originated (data not shown). Southern blot analysis of genomic DNA probed with ^{32}P-labeled *Apaf-1* cDNA revealed no differences in the gene structure of *Apaf-1* between *fog/fog* and C3H/HeJ wild-type mice (data not shown). Additionally, no differences between the C3H/HeJ background and the *fog* mutant allele were found in 2,700 base pairs of the promoter region or the 3′ untranslated region (National Center for Biotechnology Information Nucleotide query, NM_009684) of the *Apaf-1* gene. However, one primer pair that was used to amplify the coding sequence between exons 2 and 4 of *Apaf-1* (containing the first exon of its ced-4 homology domain) from *fog/fog* first strand cDNA produced a predominant PCR fragment that was ≈1,750 bp larger than the predicted size (Fig. 5 *A* and *B*). The 2-kb fragment was sequenced and found to include the intron between exons 3 and 4 of the *Apaf-1* gene (Fig. 5*D*). Because no mutations were found at the splice acceptor or donor sites flanking exons 3 and 4 or the intron between these two exons in the *fog* mutants; defective *Apaf-1* mRNA processing appears to be the cause of the markedly reduced *Apaf-1* message, protein levels, and activity in *fog* mutants (Fig. 4).

To address the possibility that a gene adjacent to *Apaf-1* that regulates *Apaf-1* expression was mutated in *fog* animals, mice carrying the *fog* mutation (which have a background similar to C3H/HeJ) were outcrossed to wild-type animals carrying *Apaf-1* in the BL6 background. The aberrantly sized 2-kb RT-PCR fragment was amplified from the RNA of resulting progeny, which had one *Apaf-1* allele from the *fog* mutant and one wild-type *Apaf-1* allele from the BL6 background. Two separate PCRs, differing only in the downstream primer used to amplify a 340-bp fragment located within the aberrantly sized 2-kb fragment, were then used to determine the allelic origin of the 2-kb band. A 14-bp insertion present in the third intron of *Apaf-1*

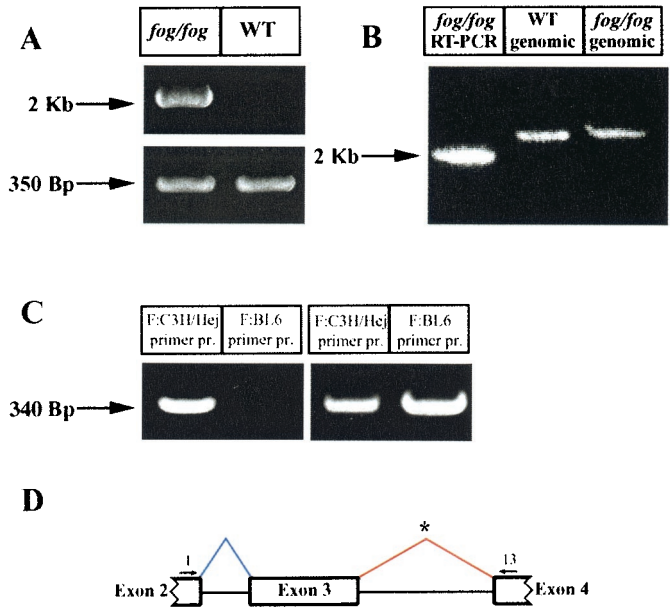

Fig. 5. Aberrant processing of the *Apaf-1* transcript in fibroblasts derived from *fog/fog* mice. When primers flanking exons 2 and 4 (primers 1 and 13) in *Apaf-1* are used, an aberrantly sized RT-PCR product is amplified (2 kb) in the *fog/fog* mutant. The 350-bp product is a β-actin positive control (shown in *A*). This fragment is smaller than the genomic fragment amplified by the same primers from wild-type or *fog/fog* DNA (shown in *B*) because it is mRNA that is partially processed. (*C*) Total RNA was prepared from the abdominal wall of mice carrying one *fog* allele (originated from the C3H/HeJ background) and one *Apaf-1* allele in the BL6 background. The genetic background of the *fog/fog* mutant possesses a 14-bp insertion in the intron between exons 3 and 4 of *Apaf-1* that is absent from the BL6 background. A common upstream primer (F, 5′-GCAAGGACACAGATGGTGGAATAAC-3′) and a pair of downstream primers (C3H/Hej, 5′-AGTTTGAGGACAGCCAGGTC-3′ or BL6, 5′-CTACAGAGTGAGTTTGTACAC-3′) designed to amplify an internal fragment within the 2-kb product were used in a PCR distinguishing the origin of the band, based on the presence or absence of the insertion. *Left* shows that the primer pair designed to include the insertion in the C3H/HeJ background preferentially amplifies the fragment. This indicates that the 2-kb band is produced by the *Apaf-1* allele in the *fog/fog* mutant, and not a separate gene that regulates *Apaf-1* expression. *Right* shows the same bands amplified from background specific DNA templates in each PCR (C3H/HeJ template in the left lane and BL6 template in the right lane). Thus, the two primer pairs are equally capable of amplifying the 340-bp fragment. (*D*) The diagram illustrates that the *fog/fog* fibroblasts splice out the intron between exon 2 and exon 3 (shown in blue), but fail to splice out the intron between exon 3 and exon 4 of *Apaf-1* (shown in red, with an asterisk).

gene of *fog* animals, but not in the BL6 wild-type mice, was used in the design of the downstream primers, such that one primer included the insertion and the other did not. The insertion found in the *fog* animals is also found in C3H/HeJ wild-type mice, indicating that the insertion is specific to the *fog* background but does not affect gene function. If the aberrant fragment resulted from a separate gene that affects *Apaf-1* expression, then PCR products with primer pairs specific for the *Apaf-1* gene in *fog* mutants and the *Apaf-1* gene in BL6 wild-type mice would both be amplified. In Fig. 5*C* it is shown that only the primer including the insertion (specific to the *Apaf-1* gene from *fog* mice) amplifies the 340-bp fragment located within the aberrant 2-kb band. This observation strongly suggests that the 2-kb band originates from the *fog* mutant allele and that the band is specific for the *Apaf-1* gene rather than the result of a mutation in another gene affecting the expression of *Apaf-1* in *fog/fog* mice.

Discussion

Residual *Apaf-1* expression likely prevents normal neural tube closure in *fog/fog* mice. The *fog* mutation, although not yet

defined on the nucleotide level, maps within the minimal region of mouse chromosome 10 containing *Apaf-1*, causes inefficient splicing of at least one intron in the *Apaf-1* gene (the third intron) in a manner that is specific to the *Apaf-1* gene in *fog* mutants, and results in dramatically reduced expression of *Apaf-1* at the level of mRNA and protein. Furthermore, the *fog* mutation abolishes detectable Apaf-1 activity *in vitro* and is able to complement one disrupted *Apaf-1* allele in producing a full *Apaf-1* mutant phenotype *in vivo*. These results are most consistent with the fog mutation as single defect in the *Apaf-1* gene and the critical neurodevelopmental role shown for *Apaf-1*.

Previous work has shown that modifier genes can vary the phenotype of *Apaf-1*-deficient mice, depending on their genetic background (9). Thus, the phenotypic differences between the *fog* mutant and the *Apaf-1* mutants generated by targeted disruption are likely because of differences in the activity of modifier genes between the two mutant models and the low, residual *Apaf-1* expression in the *fog* mutants that is not seen in *Apaf-1* knockouts. In Fig. 4, *fog* mutants are shown to have markedly reduced levels of normal *Apaf-1* message. This situation contrasts with the mutation in the *Apaf-1* knockout, in which no normal message is produced. The enhanced survival of *fog* mutants over *Apaf-1* knockout mice is best explained by the presence of residual *Apaf-1* message. However, the frequent lumbosacral defects seen in *fog* mutants (derived in the C3H/HeJ background) but not in *Apaf-1* knockouts (derived in the 129/BL6 background) is most likely the result of background differences. *Apaf-1* mutants in a 129/BL6 mixed background possessing both forebrain defects and lumbosacral defects have been infrequently obtained (data not shown), although such defects in *Apaf-1* knockouts derived in other strains have not been reported. Specifically, *Apaf-1* mutant embryos in the 129/BL6 mixed background show exencephaly, cranioschesis, anencephaly, and lumbosacral defects in combination with exencephaly, whereas *fog/fog* mutant embryos have similar defects alone as well as in combination with exencephaly or cranioschesis. The common thread in all of the reported embryonic phenotypes is the failure of appropriate neural tube closure, which has been formally demonstrated in both *Apaf-1* mutants and *fog/fog* mutants (3, 5, 8, 9). Given that both adult *Apaf-1*-deficient males and adult *fog/fog* males are infertile, the significant phenotypic overlap seen between *Apaf-1* and *fog/fog* mutants suggests that fog mutants have a defect in *Apaf-1* expression. However, the differences in the location of the neural tube closure defects between these two animal models may indicate either that an additional mutation exists in the *fog/fog* mice, which is revealed only in the presence of a particular genetic complement or reduced *Apaf-1* expression, or that genetic modifiers on the background strain of the *fog* mutant enhance the effect of the *Apaf-1* mutation on posterior neuropore closure thereby increasing the incidence of spina bifida. Based on the biochemical and genetic information presented, we conclude that the *fog* mutation is most likely a mutation in the *Apaf-1* gene (identification of the mutation at the nucleotide level is required to make the conclusion with full certainty). The mutation affects the splicing of the third intron and the efficiency of *Apaf-1* mRNA processing. Because an aberrantly sized 2-kb product was specifically amplified from the *Apaf-1* gene in the *fog* mutant, we interpret the virtually absent expression of *Apaf-1* mRNA found in *fog/fog* tissues as an indicator of significant *Apaf-1* transcript degradation that is the result of the reduced splicing efficiency.

A recent report has shown that decreased *Apaf-1* expression, as a result of DNA methylation, contributes to the pathogenesis of malignant melanoma (16). Here it is shown that reduced *Apaf-1* expression because of aberrant *Apaf-1* mRNA processing exists in *fog* mutant mice, which have spina bifida and survive to adulthood with neural tube closure defects. We also show that *Apaf-1* deficiency can result in anencephaly. Thus, mutations affecting the expression levels of Apaf-1 or other proteins in the cytochrome-*c*-mediated apoptotic cascade (such as caspases-9 and -3) may play a fundamental role in the pathogenesis of spina bifida, because anencephaly and spina bifida are often present concurrently in human subjects (see Online Mendelian Inheritance in Man, Entry 182940, http://www3.ncbi.nlm.nih.gov/Omim/). As the cytochrome-*c*-mediated apoptotic pathway is critical for the death of neural progenitor cells (9), it may also be inferred that an excess of neural progenitors contributes to the pathogenesis of neural tube closure defects seen in humans.

The study of cytochrome-*c*-mediated apoptotic cell death in disease processes has been hampered by the embryonic lethality of the mutants deficient in any one of the proteins central to the cascade. Given that the *fog* mutant mice possess hypomorphic alleles of *Apaf-1* and that adult mutants are readily available to investigators, examination of cell death in disease states occurring independently of the cytochrome-*c*-mediated cascade can be completed. Fields of investigation include (but are not limited to) immune dysfunction, ischemic cell death, and carcinogenesis.

We thank Jeffrey Stark, Kristi Cala, Daphne Davis, Jeff Cormier, Lorena Avila, and Carl Sidle for their technical assistance in completing this work. We also thank Mary Barter, Lucy Rowe, and Jennifer Johanson of The Jackson Laboratory for their expertise and help with the mapping analysis. This work was supported by National Institutes of Health Grants GM57158, HL 20948, and HL 63762, the Howard Hughes Medical Institute, the Welch Foundation, and the Alzheimer Association. J.H. was an Established Investigator of the American Heart Association and Parke–Davis.

1. DeSesso, J. M., Scialli, A. R. & Holson, J. F. (1999) *Am. J. Med. Genet.* **87,** 143–162.
2. Juriloff, D. M. & Harris, M. J. (2000) *Hum. Mol. Genet.* **9,** 993–1000.
3. Harris, B. S., Franz, T., Ullrich, S., Cook, S., Bronson, R. T. & Davisson, M. T. (1997) *Teratology* **55,** 231–240.
4. Kuida, K., Zheng, T. S., Na, S., Kuan, C., Yang, D., Karasuyama, H., Rakic, P. & Flavell, R. A. (1996) *Nature (London)* **384,** 368–372.
5. Cecconi, F., Alvarez-Bolado, G., Meyer, B. I., Roth, K. A. & Gruss, P. (1998) *Cell* **94,** 727–737.
6. Hakem, R., Hakem, A., Duncan, G. S., Henderson, J. T., Woo, M., Soengas, M. S., Elia, A., Luis de la Pompa, J., Kagi, D., Khoo, W., *et al.* (1998) *Cell* **94,** 339–352.
7. Kuida, K., Haydar, T. F., Kuan, C. Y., Gu, Y., Taya, C., Karasuyama, H., Su, M. S., Rakic, P. & Flavell, R. A. (1998) *Cell* **94,** 325–337.
8. Yoshida, H., Kong, Y. Y., Yoshida, R., Elia, A. J., Hakem, A., Hakem, R., Penninger, J. M. & Mak, T. W. (1998) *Cell* **94,** 739–750.
9. Honarpour, N., Du, C., Richardson, J. A., Hammer, R. E., Wang, X. & Herz, J. (2000) *Dev. Biol.* **218,** 248–258.
10. Smith, J. L. & Schoenwolf, G. C. (1997) *Trends Neurosci.* **20,** 510–517.
11. Willnow, T. E. & Herz, J. (1994) *Methods Cell Biol.* **43,** 305–334.
12. Zou, H., Henzel, W. J., Lui, X., Lutschg, A. & Wang, X. (1997) *Cell* **90,** 405–413.
13. Liu, X., Kim, C. N., Yang, J., Jemmerson, R. & Wang, X. (1996) *Cell* **86,** 147–157.
14. Sambrook, J. & Russell, D. W. (2001) *Molecular Cloning: A Laboratory Manual* (Cold Spring Harbor Lab. Press, Plainview, New York), 3rd Ed., pp. 721–745.
15. Rowe, L. B., Nadeau, J. H., Turner, R., Frankel, W. N., Letts, V. A., Eppig, J. T., Ko, M. S., Thurston, S. J. & Birkenmeier, E. H. (1994) *Mamm. Genome* **5,** 253–274.
16. Soengas, M. S., Capodieci, P., Polsky, D., Mora, J., Esteller, M., Optiz-Araya, X., McCombie, R., Herman, J. G., Gerald, W. L., Lazebnik, Y. A., *et al.* (2001) *Nature (London)* **409,** 207–211.